J. Non-Equilib. Thermodyn.
2008 · Vol. 33 · pp. 25–45

Mesoscopic Modeling for Continua with Pores: Dynamic Void Growth in Viscoplastic Materials

Kerstin Weinberg⋆ and Thomas Böhme
Institut für Mechanik, Lehrstuhl Kontinuumsmechanik und Materialtheorie (LKM), Sekr. MS-2, Technische Universität Berlin, Einsteinufer 5, 10587 Berlin, Germany

⋆Corresponding author (kerstin.weinberg@tu-berlin.de)

Communicated by W. Muschik and C.A. Papenfuss, Berlin, Germany

Abstract

The temporal development of arbitrarily distributed voids in a viscoplastic material under different loading regimes is investigated. For this reason, we make use of a mesoscopic continuum model extending the classical space–time domain of continuum mechanics. This extended domain requires a reformulation of the classical balance equations as well as the consideration of additional constitutive quantities. Furthermore, a mesoscopic distribution function is formulated to describe the temporal evolution of different void regimes. Here, we assume a spherical shell model for the porous composites and elaborate all required steps in order to describe load-induced void growth in a metal-like matrix. We conclude with some exemplary results that confirm experimental observations of dynamical fracture.

1. Introduction

In engineering today, the question of reliability and failure of the applied materials is of increasing importance. As a consequence of severe thermal and mechanical loading, even initially homogeneous materials start to develop a certain microstructure, e.g., distortions of the metal lattice, micro-cracks and pores. A physical measure of these microscopic changes is needed in order to avoid catastrophic failure. Such microstructural evolution can efficiently be analyzed by means of the mesoscopic theory developed by Muschik et al. [1], which represents a general approach for the description of complex internally structured materials within the continuum mechanical framework.

 DOI 10.1515/JNETDY.2008.002

In [2], the authors presented a mesoscopic concept for the theoretical description of elastic bubble oscillation in soft biological tissue. This was done regarding the interest in the physical phenomena occurring during the ultrasonic treatment of kidney stones. In the present paper, we focus on *dissipative* materials in which the internal structure is characterized by a micro-void distribution. Such material defects have been observed in many technical components. Examples are (cf. [3–5]):

(1) Void growth in spallation planes, cf., Figure 1a. Voids represent the initial stage of *dynamic fracture* observable in the surface area of ductile metals during high pressure impulses. The extremely high tension within the material lead to void nucleation at internal defects, such as impurities or grain boundaries. This damage proceeds and results in fast void expansion leading to void sheets and final failure by void coalescence.

(2) The formation and growth of Kirkendall voids within the interface of solder and substrate in microelectronic packages; cf. Figure 1b. Here the Si-chips are typically fixed at the substrate (e.g., polished Cu) by means of solder materials (e.g., Sn-Ag-Cu) in which intermetallic compounds (e.g., Cu_3Sn or Cu_6Sn_5) are formed near the solder–substrate interface; Figure 1b. The so-called Kirkendall voids appear between the Cu substrate and the thin Cu_3Sn layer due to the migration of Cu atoms from Cu_3Sn into Cu_6Sn_5, which is much faster than the Sn-diffusion from Cu_6Sn_5 toward Cu_3Sn. This unbalanced Cu-Sn

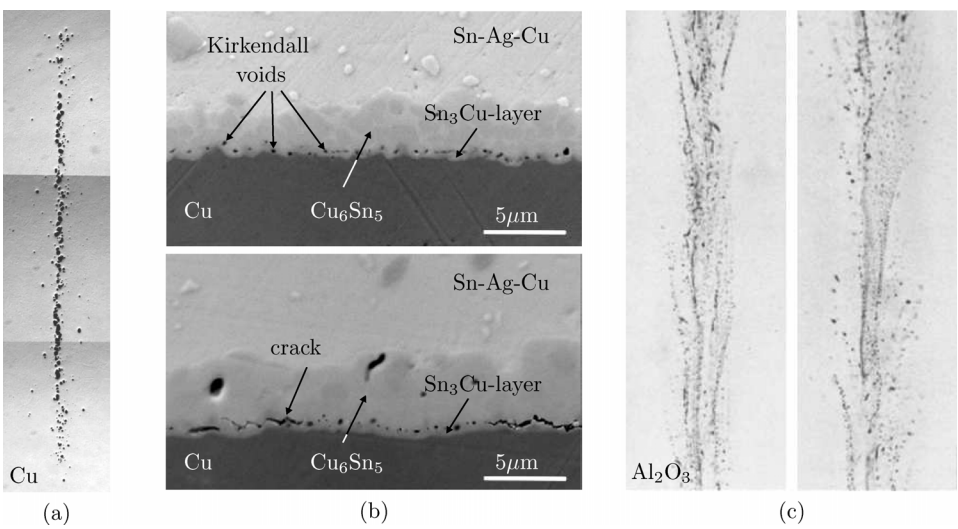

Figure 1. Technically relevant examples showing void distributions: (a) Void distribution in the spallation layer of copper [3]. (b) Kirkendall voids between solder and substrate [5]. (c) Micro-voids in sapphire filaments [4].

interdiffusion generates atomic vacancies at the lattice sites which coalesce to the Kirkendall voids; cf. [5].

(3) Micro-void formation in mono-crystal growing. Here voids grow during the crystallization process, i.e., while a crystal is pulled from the melt, bubbles of dissolved or surrounding gases may be included. The resulting void distribution depends on the growth conditions and it considerably affects the material behavior of the mono-crystal. Figure 1c illustrates a void-distribution in mono-crystalline sapphire – a widely used material in high-technology applications (e.g., in high-power lasers).

Although the origins of the voids in the presented examples are completely different, – the resulting microstructure of the materials is similar. The materials contain a certain fraction of voids separated by matrix material. Moreover, the void radii differ within a certain range and may grow in the case of external loading. Therefore, we model here the voids by an ensemble of spherical inclusion in a matrix material. This model, which will be described in detail in the next section, enables us to link the mechanisms of void expansion and global softening of the material to parameters that describe the micromechanical mechanisms in a porous solid. After a brief retrospective on the mesoscopic concept, we turn our attention in Section 3 to a constitutive model for void expansion in a material that is assumed to behave viscoplastically. In Section 4 we study different void ensembles and present numerical results. We finish with a short summary and an outlook in Section 5.

2. Model of a porous metal

In typical technical and natural materials, the pores and cavities are small compared to the size of the structure. Let their distribution within a volume element $\mathrm{d}V$ be described by the void volume fraction, $f_V(\boldsymbol{x}, t) \in \mathbb{R}$, representing the void volume per current volume at the position $\boldsymbol{x}$ and time t in the material. Here, we presume the initial void volume fraction $f_{V0} \equiv f_V(\boldsymbol{x}, t = 0)$ to be small. For engineering metals, it is in the range of $f_{V0} = 10^{-4} \ldots 10^{-2}$, cf. [6], caused, e.g., by defects in the crystal lattice or by (empty) inclusions along grain boundaries. Through straining of the material element, the pores and cavities may grow but, typically, metals fail by ductile fracture at about $f_V = 0.1 \ldots 0.3$ [6].

2.1. The spherical shell model

In order to analyze the growth of pores and cavities (voids) in a deforming solid, we imagine the material to be a conglomerate of initially very small

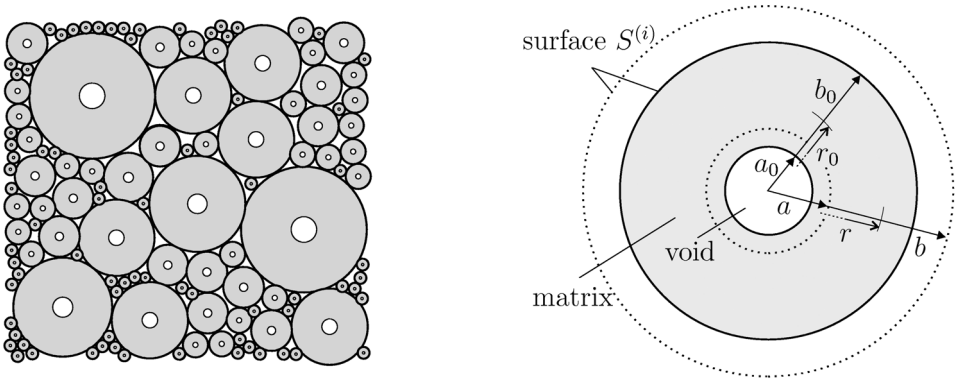

Figure 2. *Left*: Porous composite consisting of spherical shells. *Right*: Spherical shell model of a single void before and after (dashed lines) the deformation.

spherical voids each surrounded by a sphere of matrix material; see Figure 2 (left). In other words, each void i with radius $a \equiv a^{(i)}(\boldsymbol{x}, t)$ and volume $V^{(i)}_{\mathtt{void}} = (4\pi/3)\, a^3$ is at every instance completely embedded in a **spherical shell**. We exclude here the process of coalescence and it holds for each spherical shell with radius $b \equiv b^{(i)}(\boldsymbol{x}, t)$ and volume $V^{(i)}_{\mathtt{shell}} = (4\pi/3)\, b^3$,

$$\sum_i V^{(i)}_{\mathtt{shell}} = V - V_{\mathtt{rem}} \quad \text{and} \quad V^{(i)}_{\mathtt{void}} / V^{(i)}_{\mathtt{shell}} = \frac{a^3}{b^3} = f_V{}^{(i)}. \tag{1}$$

Here, V denotes the total volume and $V_{\mathtt{rem}}$ is the volume remaining between the spheres.

The porous material is now modeled as an assemblage of such spherical shells with a certain given initial void volume fraction and an initial size distribution. During the process of deformation, the spherical shells may grow (in different ways) but retain their shapes, whereas the matrix material follows classical material laws. As the remaining volume between the spheres can be made infinitesimally small, we assume, for simplicity, $V_{\mathtt{rem}} \to 0$. Then, the deformation energy of the composite body will in the limit approach the sum of deformation energies of all spherical shells.

Figure 2 (right) illustrates *one* spherical shell in its undeformed and deformed state. An arbitrary material sphere surrounding the void and deforming with the body has initial and current radii $r_0 \in [a_0, b_0]$ and $r \equiv r(t) \in [a, b]$, respectively. Presuming a volume preserving deformation, i.e.,

$$\frac{\mathrm{d}}{\mathrm{d}t}\frac{4\pi}{3}(r^3 - a^3) = 0 \quad \Rightarrow \quad r_0^3 - a_0^3 = r^3 - a^3, \tag{2}$$

gives the current radius as $r = \left(r_0^3 - a_0^3 + a^3\right)^{1/3}$. As a consequence, the current outer radius of an incompressible shell is uniquely determined by $b(a) = (b_0^3 - a_0^3 + a^3)^{1/3}$, and all subsequent equations depending on radius b can be expressed in terms of void radius a and the initial geometry. Moreover, Eq. (2) defines the deformation velocity field over the current configuration. In particular, the radial component of the spatial velocity reads

$$v_r = \frac{\mathrm{d}r}{\mathrm{d}t} = \frac{a^2}{r^2}\dot{a}, \tag{3}$$

where the rate of void radius, $\dot{a} \equiv \dot{a}(a, t) = \frac{\mathrm{d}a}{\mathrm{d}t}$, identifies the velocity of void expansion or compression, here simply denoted as **void velocity**.

2.2. Mesoscopic variables and void distribution function

The temporal change of a mass-specific quantity $\psi(\boldsymbol{x}, t)$ in a body with domain $\Omega(t)$ can be invoked by production Π^ψ and supply Σ^ψ within the body and by a flux $\boldsymbol{J}^\psi$ over the boundaries. Thus, the generic *balance equation* reads in local form (cf. [7])

$$\frac{\partial \rho\, \psi}{\partial t} + \nabla \cdot \left(\boldsymbol{v}\, \rho\, \psi + \boldsymbol{J}^\psi\right) = \Pi^\psi + \Sigma^\psi, \tag{4}$$

where ρ is the current mass density and $\boldsymbol{v}(\boldsymbol{x}, t)$ denotes the material velocity. The specific balances of mass, momentum, total and internal energy, etc., follow directly by respective the according expressions for ψ, $\boldsymbol{J}^\psi$, Π^ψ, and Σ^ψ.

The fundamental idea of the mesoscopic concept is to extend the classical space–time domain of these quantities by a set of additional parameters, the mesoscopic variables $\boldsymbol{m}$. The fields appearing in the classical balances equations are now defined on a so-called mesoscopic space $\{\boldsymbol{x}, t, \boldsymbol{m}\}$. In our case of a porous metal, the mesoscopic variables are simply the void radii $a(t)$ of the different spherical shells[1] in a volume element at position $\boldsymbol{x}$.

Additionally, a statistical function is introduced. This **mesoscopic distribution function** $\tilde{d}(\boldsymbol{m}, \boldsymbol{x}, t) \in \mathbb{R}$ describes the distribution of the mesoscopic variables: in the volume element associated with $(\boldsymbol{x}, t)$ the value of the mesoscopic variables $\boldsymbol{m}$ has fraction $\tilde{d}$ of all particles. Now the fields of mass density, momentum, total energy, etc., can be defined on the mesoscopic space.

[1] The sole use of the scalar mesoscopic variable a presumes a dependence between the radii $a(t)$ and $b(t)$ within the spherical shell ensemble as described above. A more general case could be found introducing a vectorial mesoscopic variable $\boldsymbol{m} = (a, b)$.

For distinguishing these fields from the usual, macroscopic ones and to omit the arguments in the remaining of the text, we have added a tilde to the symbol, i.e, $\tilde{\varrho} \equiv \tilde{\varrho}(\boldsymbol{m}, \boldsymbol{x}, t)$, $\tilde{\boldsymbol{v}} \equiv \tilde{\boldsymbol{v}}(\boldsymbol{m}, \boldsymbol{x}, t)$, $\tilde{e} \equiv \tilde{e}(\boldsymbol{m}, \boldsymbol{x}, t)$, and so on.

From a mathematical point of view, the mesoscopic balance equations differ from the macroscopic ones only in their domain, which is enlarged by the mesoscopic variables. Therefore, derivatives with respect to these variables now appear in the balances. Thus, the generic *mesoscopic balance equation* reads in local form (cf. [8])

$$\frac{\partial}{\partial t}\,\tilde{\rho}\,\tilde{\psi} + \nabla_x \cdot \left[\tilde{\boldsymbol{v}}\,\tilde{\rho}\,\tilde{\psi} - \tilde{\boldsymbol{J}}^{\psi,\boldsymbol{x}}\right] + \nabla_m \cdot \left[\tilde{\boldsymbol{u}}\,\tilde{\rho}\,\tilde{\psi} - \tilde{\boldsymbol{J}}^{\psi,\boldsymbol{m}}\right] = \tilde{\Pi}^{\tilde{\psi}} + \tilde{\Sigma}^{\tilde{\psi}}. \quad (5)$$

The velocity of mesoscopic change $\tilde{\boldsymbol{u}} \equiv \tilde{\boldsymbol{u}}(\boldsymbol{m}, \boldsymbol{x}, t)$ is the analog to the material velocity $\tilde{\boldsymbol{v}}$; in our model it is the void velocity $\dot{a}$ defined in Eq. (3). Moreover, derivative ∇_m stands here for $\partial/\partial a$. Mesoscopic balances of mass, momentum, and energy can now be formulated.

The mesoscopic concept does not introduce new balance for the additional fields though these are included in the mesoscopic space. However, the mesoscopic distribution function $\tilde{d}$ and the velocity of mesoscopic change $\dot{a}$ require additional equations. To specify the mesoscopic distribution function for the porous material under consideration here, let $\tilde{N}_V = \tilde{N}_V(a, \boldsymbol{x}, t)$ be the number of shells with voids of radius a in the volume element at $\{\boldsymbol{x}, t\}$. We presume that all voids have a nucleation size a_{nuc} and that the void radius is bounded by half of the characteristic length of the volume element, $l_{\text{VE}} = \sqrt[3]{\mathrm{d}V}$. Then, the total number of voids per unit volume results in

$$N_V(\boldsymbol{x}, t) = \int_{a_{\text{nuc}}}^{l_{\text{VE}}/2} \tilde{N}_V \,\mathrm{d}a, \quad (6)$$

and we define the mesoscopic **void distribution function** by

$$\tilde{d} \equiv d(a, \boldsymbol{x}, t) = \frac{\tilde{N}_V}{N_V(\boldsymbol{x}, t)} \quad \text{with normalization} \quad \int_{a_{\text{nuc}}}^{l_{\text{VE}}/2} \tilde{d}\,\mathrm{d}a = 1. \quad (7)$$

In order to obtain an evolution equation for the void distribution function, we start from Eq. (5) and formulate the balance of the mesoscopic void number density

$$\frac{\partial \tilde{N}_V}{\partial t} + \nabla_x \cdot (\tilde{N}_V \tilde{\boldsymbol{v}}) + \frac{\partial}{\partial a}\,(\tilde{N}_V \dot{a}) = \tilde{\Pi}^{\tilde{N}_V}, \quad (8)$$

where symbol $\tilde{\Pi}^{\tilde{N}_V}$ denotes a production term referring to void nucleation and/or coalescence. Because all voids are embedded in the matrix of the solid (and do not move independently), the mesoscopic velocity $\tilde{\boldsymbol{v}}$ is identical for all voids and equals the macroscopic velocity of the volume element, $\tilde{\boldsymbol{v}} = \boldsymbol{v}(\boldsymbol{x}, t)$. Multiplying Eq. (8) with $1/N_V$ and applying Eq. (7) results after a minor calculation in

$$\frac{\partial \tilde{d}}{\partial t} + \nabla_x \cdot (\tilde{d}\boldsymbol{v}) + \frac{\partial}{\partial a}\left(\tilde{d}\dot{a}\right) = \tilde{\Pi}^{\tilde{N}_V} + \frac{\tilde{d}}{N_V}\left(\frac{\partial N_V}{\partial t} + \boldsymbol{v} \cdot \nabla_x N_V\right). \quad (9)$$

The right-hand side of Eq. (9) represents two different but not independent production terms; for a discussion, see [2]. Here we neither consider void nucleation nor coalescence and these terms vanish. Thus, Eq. (9) becomes a conservation law and the *balance of the void distribution function* reads

$$\frac{\partial \tilde{d}}{\partial t} + \nabla_x \cdot (\tilde{d}\boldsymbol{v}) + \frac{\partial}{\partial a}\left(\tilde{d}\dot{a}\right) = 0. \quad (10)$$

By means of Eq. (10) the evolution of voids in a general material is predictable. For application to the specific materials we envision here, the constitutive equation for the void velocity within the ensemble, $\dot{a}(a, \boldsymbol{x}, t)$, remains to be specified.

3. Constitutive model

In what follows, we want to consider the deformation process of a volume element $\mathrm{d}V$ containing an ensemble of spherical shells. We postulate the existence of a **free energy** function $A(\boldsymbol{x}, t)$ as a weighted sum of free energy contributions of *all* spherical shells. The energy required to deform *one* shell, $\tilde{A}$, is a sum of energy contributions accompanying shell deformation and void expansion.

Exposing the spherical shell ensemble to externally applied forces, e.g., a **tension field** $p(t)$, generally invokes an inhomogeneous stress field. In this model we assume an *averaged* stress field of the form $\boldsymbol{\sigma}(a, \boldsymbol{x}, t) \doteq \boldsymbol{\sigma}$, i.e., all spherical shells "feel" the same loading.[2] Moreover, we assume the power of the external forces acting on *one* spherical shell $\tilde{P} \equiv P(a, \boldsymbol{x}, t)$ to be completely compensated by the rate of free energy,

$$\tilde{P} = p(t) \cdot \frac{\mathrm{d}\tilde{V}_{\mathrm{shell}}}{\mathrm{d}t} = \frac{\mathrm{d}\tilde{A}}{\mathrm{d}t}. \quad (11)$$

[2] This assumption is established in the field of homogenization as the Reuss approximation [9].

With a specified right-hand side and with initial values a_0 and b_0, Eq. (11) represents a differential equation for the void radius in one spherical shell. Solving this equation for all voids with different initial conditions yields a constitutive relation for the void velocity in Eq. (3).

Let us now specify the constitutive equations for a viscoplastic material with *three* contributions to the free energy function: (1) energy required for plastic deformation of the matrix material $\tilde{W}^p$, (2) kinetic energy $\tilde{K}$ of void expansion, and (3) surface energy $\tilde{S}$ stored in the interface between void and matrix.

3.1. Stored plastic work

Exploiting the spherical symmetry of the model and the plastic incompressibility constraint of the matrix material we can derive from the kinematics outlined in Section 2 the principle stresses and strains within one shell. Correspondingly, the velocity over the current configuration (3) yields the strain rate as

$$\dot{\varepsilon}(r,t) = \frac{\partial \dot{r}}{\partial r} = -\frac{2a^2(t)}{r^3(t)}\,\dot{a}(t). \tag{12}$$

The absolute value of strain rate (12) defines the rate of the effective von Mises strain, $\dot{\varepsilon^p} \equiv |\dot{\varepsilon}(r,t)|$. Presuming a monotonic void growth, i.e., $\dot{a}(t) > 0$, $(\forall t)$, Eq. (12) can be integrated to give

$$\varepsilon^p = \left| -\int_0^t \frac{2a^2\dot{a}}{\dot{r}}\,\mathrm{d}\tau \right| = \left| -\frac{2}{3}\log\left(1 + \frac{a^3 - a_0^3}{r^3 - (a^3 - a_0^3)}\right) \right|$$

$$= \frac{2}{3}\log\left(1 + \frac{a^3 - a_0^3}{r_0^3}\right). \tag{13}$$

Let us consider the classical von Mises plasticity with power law hardening of the yield stress σ_y,

$$\sigma_y = \sigma_0\left(1 + \varepsilon^p/\varepsilon_0^p\right)^{1/n}, \tag{14}$$

where $n \in [1,\infty)$ denotes the hardening exponent and σ_0, ε_0^p are the initial yield stress and a reference plastic strain, respectively. With $n = 1$ we prescribe linear isotropic hardening, whereas $n \to \infty$ enforces perfect plasticity. Additionally, one may include here a temperature dependence of the yield

stress, $\sigma_0(T)$; cf. [10]. The stored plastic energy density follows from the rate of plastic straining by

$$\int_0^t \sigma_y \dot{\varepsilon^p}\ \mathrm{d}\bar{t} = \int_{\varepsilon_0^p}^{\varepsilon^p} \sigma_y\ \mathrm{d}\bar{\varepsilon^p} = \varepsilon_0^p \sigma_0(T) \frac{n}{n+1} \left[\left(1 + \frac{\varepsilon^p}{\varepsilon_0^p} \right)^{\frac{n+1}{n}} - 1 \right]. \quad (15)$$

A volume integration results in the stored plastic energy of one spherical shell:

$$\tilde{W}^{\mathrm{p}}(a, b; T, n) = \int_a^b \varepsilon_0^p \sigma_0(T) \frac{n}{n+1} \left[\left(1 + \frac{\varepsilon^p}{\varepsilon_0^p} \right)^{\frac{n+1}{n}} - 1 \right] 4\pi r^2\ \mathrm{d}r. \quad (16)$$

Note that the result of (16) does not depend on the radius r. Evaluating (16) with (13) and substituting $x := r^3/a^3$ gives

$$\tilde{W}^{\mathrm{p}}(a, b; T, n) = \varepsilon_0^p \sigma_0(T) \frac{n}{n+1} \frac{4\pi a^3}{3} \int_0^{b^3/a^3} \left(1 + \frac{2}{3\varepsilon_0^p} \log \frac{x}{x - 1 + a_0^3/a^3} \right)^{\frac{n+1}{n}} \mathrm{d}x. \quad (17)$$

By means of relation (2) the dependence of $\tilde{W}^p$ on radius b can be eliminated and we obtain

$$\tilde{W}^{\mathrm{p}} = \tilde{W}^{\mathrm{p}}(a; T, n) = \varepsilon_0^p \sigma_0 \frac{n}{n+1} \frac{4\pi {a_0}^3}{3} g(a; n), \quad (18)$$

$$g(a; n) = \int_0^{b_0^3/a_0^3} \left\{ 1 + \frac{2}{3\varepsilon_0^p} \log \left[1 + \frac{1}{x} \left(\frac{a^3}{{a_0}^3} - 1 \right) \right] \right\}^{\frac{n+1}{n}} \mathrm{d}x. \quad (19)$$

The stored energy function (18) is attributed directly to the growth of one void of radius a. The *total* stored plastic energy can be calculated by the "weighted sum" over the individual spherical shells using the mesoscopic distribution function (10). It reads

$$W^{\mathrm{p}}(\boldsymbol{x}, t) = \int_{a_{\mathrm{nuc}}}^{l_{\mathrm{VE}}/2} \tilde{d} \tilde{W}^{\mathrm{p}}\ \mathrm{d}a. \quad (20)$$

3.2. Kinetic energy

In an analogous manner, the kinetic energy of an expanding void ensemble can be determined. With the radial component of spatial velocity (3) the kinetic

energy of *one* expanding void is computed to be

$$\tilde{K} = \tilde{K}(a, \dot{a}) = \int_V \frac{1}{2}\,\varrho \tilde{\boldsymbol{v}}^2 \mathrm{d}V$$

$$= \int_a^b \frac{1}{2}\,\varrho_0\, v_r^2\, 4\pi r^2\ \mathrm{d}r = 2\pi\,\varrho_0\, a^4 \left(\frac{1}{a} - \frac{1}{b}\right) \dot{a}^2, \qquad (21)$$

where ϱ_0 denotes the mass density of the matrix material which is constant because of plastic incompressibility, and $b = b(a)$. Then, analogously to Eq. (20), the *total* kinetic energy of the porous ensemble follows as

$$K(\boldsymbol{x}, t) = \int_{a_{\mathrm{nuc}}}^{l_{\mathrm{VE}}/2} \tilde{d}\tilde{K}\ \mathrm{d}a. \qquad (22)$$

3.3. Surface energy

The surface energy $\tilde{S}$ in the interface of *one* void with radius a as well as the according *total* surface energy of the whole ensemble are determined by the relations

$$\tilde{S} := S(a) = 4\pi a^2 \gamma \qquad \text{and} \qquad S(\boldsymbol{x}, t) = \int_{a_{\mathrm{nuc}}}^{l_{\mathrm{VE}}/2} \tilde{d}\tilde{S}\ \mathrm{d}a, \qquad (23)$$

where γ denotes the surface tension (in [N/m]).

3.4. External power and governing differential equation

With Eq. (11) and the kinematics of Section 2, the external power of a spherical shell results in $\tilde{P} = p(t) \cdot \mathrm{d}_t \left(\frac{4}{3}\pi (b_0^3 - a_0^3 + a^3)\right)$. Consequently, we write for $\tilde{P}$ and for the macroscopic power P consumed by the whole spherical shell ensemble

$$\tilde{P} = p(t) \cdot 4\pi a^2 \dot{a} \quad \text{and} \quad P(\boldsymbol{x}, t) = \int_{a_{\mathrm{nuc}}}^{l_{\mathrm{VE}}/2} \tilde{d}\tilde{P}\ \mathrm{d}a. \qquad (24)$$

Inserting the expressions (18), (21), $(23)_1$, and $(24)_1$ into ansatz (11) results in

$$
\begin{aligned}
0 &= \tilde{P} - \frac{\mathrm{d}}{\mathrm{d}t}\left(\tilde{W}^{\mathrm{p}} + \tilde{K} + \tilde{S}\right) \\
&= p(t)\cdot a^2\dot{a} \;-\; \varepsilon_0^p \sigma_0 \frac{n}{n+1}\frac{a_0^3}{3}\dot{g}(a;n) \;-\; 2a\gamma\,\dot{a} \\
&\qquad - \frac{\rho_0}{2}\left[2\ddot{a}\dot{a}a^3 + 3\dot{a}^3a^2 - \frac{a^3}{b}\left(2\ddot{a}\dot{a}a + 4\dot{a}^3 - \frac{a^3\dot{a}^3}{b^3}\right)\right],
\end{aligned}
\tag{25}
$$

where we abbreviate $b = (b_0^3 - a_0^3 + a^3)^{1/3}$. This ordinary differential equation can be solved (numerically) for *every* shell of radius $a(t)$ and of known initial geometry, $a_0 = a(t = 0)$ and $b_0 = b(t = 0)$. Once the values of void velocity $\dot{a}$ have been found for *all* different shells, the evolution of the void size distribution function can be solved by means of Eq. (10).

4. Analysis of void ensembles

In an attempt to illustrate the capability of the constitutive model derived in the previous section, we now analyze void growth for a typical metal with the material data of Table 1. In the following, we consider a volume element at fixed spatial position $\boldsymbol{x}$, i.e., $\mathrm{d}V = \mathrm{d}V(t)$, subjected to different loading regimes $p(t)$. Note that a positive value of $p(t)$ refers to hydrostatic tension.

Table 1. Material parameters representative of aluminum. The following units are chosen: Young's modulus E in [GPa], Poisson's ratio ν in [-] (dimensionless), mass density ϱ in [kg/m^3], initial yield stress σ_0 in [MPa], reference plastic strain ε_0^p in [-], surface tension γ in [N/m], and hardening exponent n in [-].

E	ν	ϱ	σ_0	ε_0^p	γ	n
69	0.33	2700	80	0.0012	5	10

4.1. Growth of equally sized voids under hydrostatic tension

We start with the special case of a void ensemble with an average radius of size $\bar{a}$, i.e., the initial void distribution function $\tilde{d}(t = 0)$ has the form of a dirac impulse at $\bar{a}_0$ and remains this shape for the expanding voids of radius $\bar{a} \geq \bar{a}_0$; for ease of reading, we write $a \equiv \bar{a}$.

4.1.1. Quasistatic void growth In case of a slow loading regime, the effect of inertia can be neglected. Assuming a constant remotely applied tension $\bar{p}$, we get from Eq. (25)

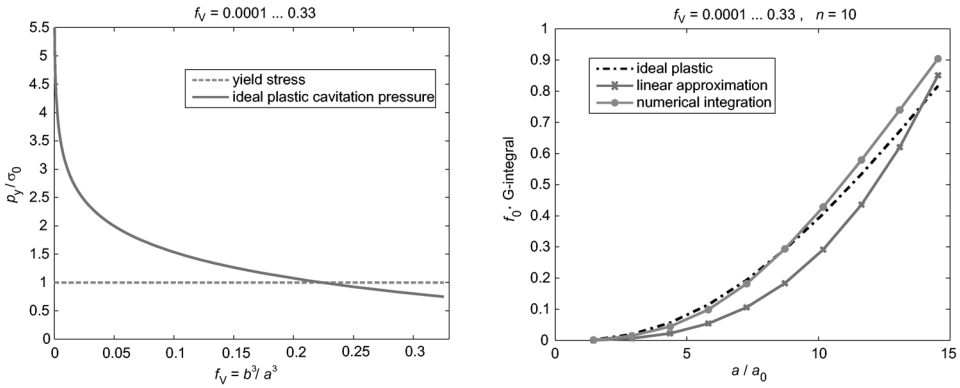

Figure 3. *Left:* Perfect plastic cavitation pressure depending on void volume fraction f_V in a quasistatic regime. *Right:* Solution and approximation of Eq. (19) muliplied by $(1.5\varepsilon_0^p)^{-(n+1)/n}$.

$$\tilde{P} = \frac{\mathrm{d}}{\mathrm{d}t}\left(\tilde{W}^p + \tilde{S}\right) \quad \Rightarrow \quad \bar{p}a^2 = \frac{n\sigma_0\varepsilon_0^p}{n+1}\frac{{a_0}^3}{3}\, g'(a;n) + 2a\gamma\,, \tag{26}$$

where $g'(a;n)$ denotes the derivative of integral (19) w.r.t. radius a. Solving the plastic energy term of $(26)_2$ for the special case of perfect plasticity, i.e., $n \to \infty$, and dividing the expression by a^2 results in

$$\bar{p} = \frac{2\sigma_0}{3}\left(\log(a^3 - a_0^3 + b_0^3) - \log(a^3)\right) + \frac{2\gamma}{a}. \tag{27}$$

Equation (27) defines an algebraic relation between applied tension $\bar{p}$ and void radius a. Note that we neglect in our constitutive model any elastic void expansion. In consequence, Eq. (27) is actually an inequality determining a critical tension necessary to induce a void to grow plastically. This corresponds to the concept of critical **cavitation pressure** as discussed, e.g., in [11–13]:

$$\bar{p} \geq p_y = \frac{2\sigma_0}{3}\log\left(1 + \frac{b_0^3 - a_0^3}{a^3}\right) + \frac{2\gamma}{a} \quad \text{(cond. for void expansion)} \tag{28}$$

The material-specific critical cavitation pressure depends on initial and current void volume fraction. For a perfect plastic material, Eq. (28) defines a high initial cavitation pressure, which considerably softens immediately after the voids start to grow; see Figure 3 (left). For a hardening material, the slope is smaller, i.e., the cavitation pressure reduces more slowly with rising void size.

In general, an analytical expression for p_y cannot be obtained because the integral of Eq. (19) is trackable by analytical means only for $n \to \infty$. If a

repeated numerical solution of Eq. (19) for every value of a is too cumbersome, we suggest here a simple linear approximation:

$$g(a;n) \approx h_n \left(\frac{2}{3\varepsilon_0^p}\right)^{\frac{n+1}{n}} \left(\frac{a^3}{a_0^3} - 1\right), \tag{29}$$

where h_n is a constant depending on hardening exponent n. This constant needs to be fitted to the values of integral (19), once numerically evaluated over a range of realistic (initial and final) void volume fractions; see Figure 3 (right). We proceed here with $h_n = 2.21$ for $n = 10$ and $f_{V0} = 10^{-4}$. Note that the approximation (29) may also provide a way to fit the critical cavitation pressure to values known from experiments, if available.

Assuming from now on a hypercritical tension $\bar{p}$, let us discuss void growth in a quasistatic regime, Eq. (27). The yield stress of a material, usually in the range of some MPa, weights the first term in Eq. (27) much stronger than the surface tensions; cf. Table 1. This effect is compensated by factor $1/a$ for very small void sizes. Only if the void is near vacancy size (0.5–50 nm) does the surface energy contribute significantly to void growth. Otherwise, the second term in Eq. (27) is negligible.

In consequence, we approximate the initial cavitation pressure for void expansion in a perfect plastic and in a hardening material ($n \in \mathbb{N}$) by

$$p_{y0} = \frac{2\sigma_0}{3} \log\left(\frac{b_0^3}{a_0^3}\right) \quad \text{and}$$

$$p_{y0} = \frac{n\,\sigma_0\,\varepsilon_0^p\,a_0^3}{3(n+1)a^2}\,g'(a;n) \;\approx\; \frac{n\,\sigma_0 \varepsilon_0^p h_n}{n+1}\left(\frac{2}{3\varepsilon_0^p}\right)^{\frac{n+1}{n}}, \tag{30}$$

respectively.

4.1.2. Dynamic void growth in a perfect plastic material In a next step, we extend the above relations to dynamic loading regimes with a constant but hypercritical tension $\bar{p} > p_{y0}$. Integrating Eq. (25) in the interval $[0, t]$ and inserting Eq. (30) yields

$$\frac{1}{3}\bar{p}(a^3 - a_0^3) = \frac{1}{3}p_{y0}(a^3 - a_0^3) + \gamma\,(a^2 - a_0^2) + \frac{1}{2}\varrho_0\,a^4\left(\frac{1}{a} - \frac{1}{b}\right)\dot{a}^2. \tag{31}$$

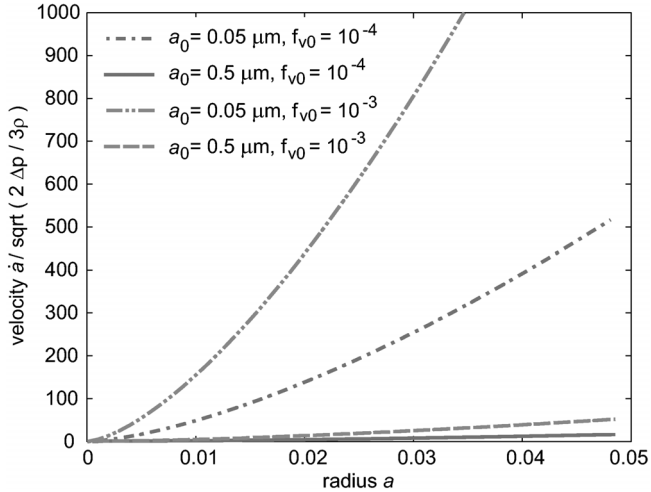

Figure 4 Velocity of void expansion as a function of radius a for different initial data.

Evaluating this ODE of first order in $a(t)$ gives

$$\dot{a} = \sqrt{\frac{2}{3\varrho_0}}\ \left(\bar{p} - p_{y0} - p_\gamma\right)^{\frac{1}{2}}\ \left(\frac{1-(a_0^3/a^3)}{1-(a/(a^3+b_0^3-a_0^3)^{1/3})}\right)^{\frac{1}{2}}, \qquad (32)$$

where $p_\gamma = 3\gamma\,(a^2 - a_0^2)/(a^3 - a_0^3)$ is the term resulting from surface energy contributions, which has significance only at the beginning of the void growth process when $a \gtrsim a_0$. By the presumption of hypercritical loading, the pressure difference is $\Delta p \equiv \bar{p} - p_{y0} - p_\gamma > 0$ and the second term of Eq. (32) is positive. Moreover, it is clear from Eq. (32) that the void velocity reduces for high density materials, whereas a small value of ϱ_0 allows the voids to grow faster. The solution of Eq. (32) is displayed in Figure 4 for $\varrho_0 = 2/3$, $\Delta p = 1$ and some realistic initial void sizes. Note that, although the applied tension $\bar{p}$ is constant, the void velocity increases unboundedly with rising void size.

Some particular cases merit special attention:

I: $b_0 \to \infty$**.** This case corresponds to a void of radius a_0 in an infinite matrix as analyzed in [12]. Equation (32) becomes

$$\dot{a} = \sqrt{\frac{2}{3\varrho_0}}\ \left(\bar{p} - p_{y0} - p_\gamma\right)^{\frac{1}{2}}\ \left(1 - \frac{a_0^3}{a^3}\right)^{\frac{1}{2}}, \qquad (33)$$

with the third term $\in [0, 1)$. In this case (and only in this case), the void expansion velocity is bounded.

II: $b_0 \to \infty, a_0 \to 0$**.** For a very small void in an *infinite* matrix the void expansion velocity is constant, namely

$$\dot{a} = \sqrt{\frac{2}{3\varrho_0}} \left(\bar{p} - p_{y0} - p_\gamma\right)^{\frac{1}{2}}. \tag{34}$$

4.1.3. Dynamic void growth in a hardening material Next we analyze void expansion in a volume element of viscoplastic material with hardening subjected to hydrostatic tension. Evaluating Eq. (25) for the void acceleration $\ddot{a}$ gives

$$\ddot{a} = \left\{ \frac{1}{\rho_0} \left[\bar{p}a^2 - 2a\gamma - \frac{n a_0^3 \varepsilon_0^p \sigma_0}{3(n+1)} g'(a;n) \right] \right.$$
$$\left. - \dot{a}^2 \left(\frac{3a^2}{2} - \frac{2a^3}{b} + \frac{a^6}{2b^4} \right) \right\} \times \left(a^3 - \frac{a^4}{b} \right)^{-1}.$$

In order to determine $a(t)$, $\dot{a}(t)$, and $\ddot{a}(t)$, this equation is solved numerically by recourse to a Runge–Kutta scheme with adapted time step. The derivative of integral (19) w.r.t. a, $g'(a;n)$, is computed numerically (no approximation in the sense of Eq. (29) is performed). The initial conditions are $a_0 = 25$ µm and $f_{V0} = a_0^3/b_0^3 = 10^{-4}$.

Applying instantaneously a constant tension of 1 GPa, we compute the results displayed in Figure 5. A population of voids expands, and, despite the hardening material, we observe an increase of void radius, of void velocity, *and* of void acceleration up to the theoretical limit of $f_V = 1$. Note that this "self-accelerating" void expansion is equivalent to a *macroscopic softening* of the composite material.

In general, the dynamic void expansion is faster, the smaller the initial voids are. The surface energy retards void growth in the first stages, superposed by a significant effect of inertia. The initial void volume fraction is of small influence, but generally the void growth decelerates with lower values of f_{V0}; cf. comments in Section 4.1.2.

4.1.4. High pressure impulse Let us apply now a sinusoidal pressure impulse with an amplitude of 10 GPa within a short time interval of $t_{load} = 1$ ns. A void ensemble with $a_0 = 0.1$ µm expands to $a = 1.57$ µm at $t = t_{load}$. The corresponding void volume fraction rises from $f_{V0} = 10^{-4}$ to $f_V = 0.28$. Starting with the same initial void volume fraction but a smaller void size

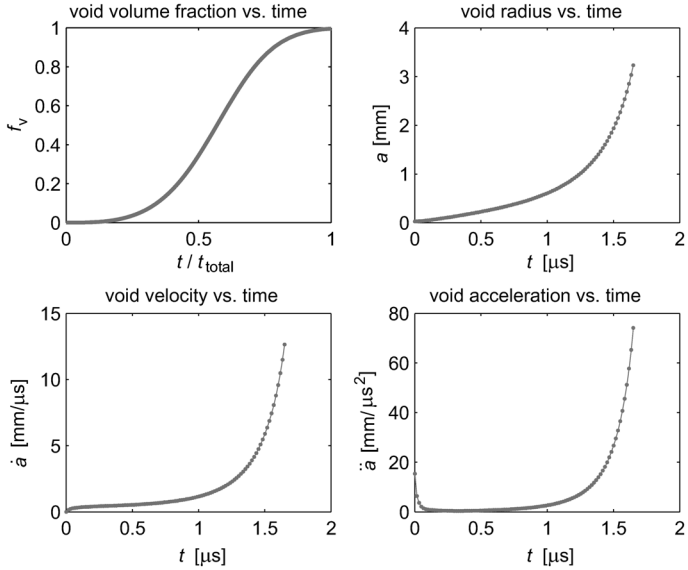

Figure 5 Void growth of an equally sized void ensemble under constant tension.

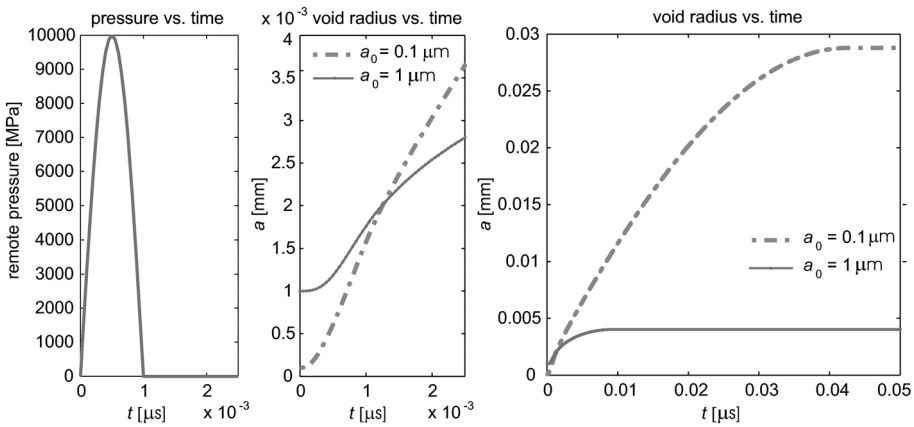

Figure 6. Inertia-dominated void growth due to a pressure impulse for two different radii, short-term and long-term response.

increases the void expansion. In particular, we observe a dependence of the form $\dot{a}(t) \propto (\sqrt{\bar{p}}/a_0)$ for $t \in [0, t_{load}]$.

The void expansion is here clearly dominated by inertia effects. This is nicely illustrated in Figure 6, where we see that the voids continue to grow after the load impulse has passed, i.e., for $\bar{p} = 0$, $t > t_{load}$. For $a_0 = 0.1$ μm the final void volume fraction reaches $f_V \to 1$. Starting with bigger voids of $a_0 = 1$ μm the void velocity and size increase are smaller, $a(t = t_{load}) = 1.76$ μm, and

the void growth converges to a final void size of $a = 4.03\ \mu\text{m}$. This regime of inertia-dominated void growth is of particular importance for impact and spallation problems; see, e.g. [11, 13–15].

4.2. Analysis of void size distribution

After studying the principles of void growth, we proceed with an ensemble of differently sized voids. Point of departure is the balance of the void distribution function (10), where we additionally assume that the body is not in motion, $\boldsymbol{v} = 0$.

Let the initial number of voids $\tilde{N}_V(a, t = 0)$ be given by a Gaussian distribution around an initial mean radius $\bar{a}_0$,

$$\tilde{N}_V(a, t = 0) = \tilde{N}_V(a_0) = c_0 \mathrm{e}^{-\frac{1}{2}\left(\frac{a_0 - \bar{a}_0}{\bar{a}_0 \epsilon_0}\right)^2}, \tag{35}$$

where c_0 is a normalization factor, ϵ_0 denotes the deviation (the "width" of distribution), and an index $\cdot_0$ refers to the initial configuration. By means of Eq. (6), the initial number of particles N_{V0} can be obtained. Introducing an integration variable $x = (a_0 - \bar{a}_0)/(\epsilon_0 \bar{a}_0 \sqrt{2})$, we get

$$\begin{aligned} N_{V0} &= \int_0^\infty \tilde{N}_V(a_0)\, \mathrm{d}a_0 \\ &= \epsilon_0 \bar{a}_0 c_0 \sqrt{2} \int_{-1/(\epsilon_0\sqrt{2})}^{\infty} \mathrm{e}^{-x^2} \mathrm{d}x \overset{(\epsilon_0 \ll 1)}{\cong} \epsilon_0 \bar{a}_0 c_0 \sqrt{2\pi} \end{aligned} \tag{36}$$

to determine c_0; the approximation refers to small values of a_0 and $\epsilon_0 \ll 1$. With Eq. (7), the initial void distribution function reads

$$\tilde{d}_0 = \frac{c_0}{N_{V0}} \cdot \mathrm{e}^{-\frac{1}{2}\left(\frac{a_0 - \bar{a}_0}{\bar{a}_0 \epsilon_0}\right)^2} \approx \frac{1}{\epsilon_0 \bar{a}_0 \sqrt{2\pi}} \cdot \mathrm{e}^{-\frac{1}{2}\left(\frac{a_0 - \bar{a}_0}{\bar{a}_0 \epsilon_0}\right)^2}. \tag{37}$$

The problem of interest is now, how does this distribution change in time? We start by discretizing the void distribution function for void radius a

$$\begin{aligned} \delta\tilde{d}(a, t) = \lim_{\Delta a \to 0} \Big(\tilde{d}(a + \Delta a, t) - \tilde{d}(a, t) \Big) \\ \wedge \quad \Delta\tilde{d}^{(i)}(t) = \tilde{d}(a^{(i)} + \Delta a, t) - \tilde{d}(a^{(i)}, t), \end{aligned}$$

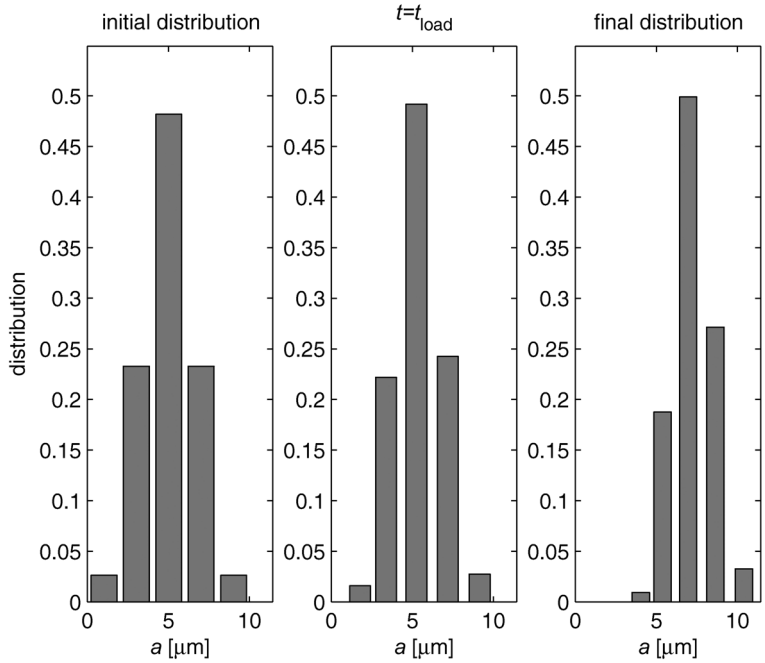

Figure 7 Initial, intermediate, and final distribution in a void ensemble of five sizes.

where $\tilde{d}^{(i)}$ is the distribution of voids with radii $a \in [a^{(i)}, a^{(i)} + \Delta a]$. Furthermore, it holds

$$1 = \int_{a_{\text{nuc}}}^{l_{\text{VE}}/2} \tilde{d}(a,t)\mathrm{d}a \;\approx\; \sum_{i=1}^{n} \tilde{d}^{(i)}. \tag{38}$$

Exemplarily, we analyze a volume element with an ensemble of five voids ($N_V = N_{V0} = 5$), with an initial void volume fraction of $f_{V0} = 10^{-4}$ and with $a_0^{(1)} = 1$ μm, $a_0^{(2)} = 3$ μm, $a_0^{(3)} = 5$ μm, $a_0^{(4)} = 7$ μm, $a_0^{(5)} = 9$ μm. The volume element is subjected to the sinusoidal loading impulse of Figure 6 with $p_{\max} = 10$ GPa and $t_{\text{load}} = 1$ ns. With the parameter $\bar{a}_0 = 5$ μm, $\epsilon_0 = 1/3$, $c_0 = N_{V0}/(\bar{a}_0\,\epsilon_0\sqrt{2\pi})$ and Eq. (37), the initial (discrete) distribution function $\tilde{d}_0^{(i)}$ is obtained; see Figure 7 (left).

As outlined in Section 4.1, we determine the mesocopic void velocities $\dot{a}^{(i)} = \dot{a}(a^{(i)}, t)$ to solve Eq. (10). Figure 7 shows the numerical solution using a Runge–Kutta scheme with time step $\Delta t \leq 10^{-11}$s. Subjected to the loading impulse, all voids grow. From the analysis of Section 4.1, we know that voids with small initial size are less inert and grow faster than their bigger companions. Consequently, the change of distribution function $\tilde{d}$ is not symmetric.

The set of small voids reduces, whereas the numbers of bigger void sizes grow.

As a consequence of the inertial effects, the void distribution keeps changing after the actual loading time passes. Therefore, the initial distribution, the distribution at the end of the impulse $t = t_{load}$, and the final distribution after 20 µs are displayed.[3] Again, the fraction of bigger voids grows. This observation is in agreement with other theories of multi-phase materials (as, e.g., Ostwald ripening and the LSW[4] theory for liquid droplets in a gas; cf. [16]) where the bigger inclusions grow at the cost of the smaller ones.

Figure 7 already indicates that the inertial effects result is a smaller variety of void sizes, i.e., the "width" of distribution function $\tilde{d}$ gets smaller. This trend has been supported by numerical studies of more different voids (e.g., 10 or 30 different radii). The effect may explain some of the difference between static and dynamic fracture of ductile metals. Whereas in static experiments we usually observe a cup-cone-like fracture with large plastic straining and small and big (coalesced) voids, in dynamic experiments the fracture surface is more or less plain but dimpled. Voids of similar sizes grew here and set up sheets of voids resulting in fragmented surfaces, e.g., spallation planes, see Figure 1a.

5. Conclusions

In our paper, we have explained a mesocopic continuum model as well as an approach for the required material relations in order to describe the temporal development of a certain void distribution in an viscoplastic material. Moreover, in the foregoing sections, exemplarily results were illuminated for different loading regimes and the evolution of five different voids under a short pressure impulse was presented.

Although the physical background, the assumptions, and the interpretations of the results are completely different, one can recognized similarities to the equations of so-called LSW theories. So, in both theories, the central element is the distribution function, which characterizes the temporal development of the number of "inclusions" with a certain radius. This equation is usually defined ad hoc, whereas we derive this equation in the mesoscopic framework. Moreover, the resulting balance of the mesoscopic void distribution is more generally admitted, because it contains a production term on the right-hand side and does not presume a constant volume fraction. Thus, it is possible to describe an increasing void volume as well as nucleation and coalescence

[3] Note that the width of the bars in Figure 7 has no meaning.

[4] LSW stands for the initials of the pioneers in this research: I.M. Lifshitz, V.V. Slyozov, and C. Wagner.

of voids. However, both theories qualitatively show the same asymmetrical temporal development of the distribution function (indicated by different void velocities) but differ in the employed constitutive relation (LSW revert to the Gibbs–Thomson equation).

Various questions and tasks are open or under current investigation, respectively. So, it would be interesting to consider the behavior of voids in an elastic-plastic material. Furthermore, the question of the definition of a macroscopic damage parameter arises, characterizing, e.g., a current averaged void radius and its consequences on the classical (macroscopic) material laws. This parameter may be very similar to the damage parameter for soft tissue presented in [2]. Finally, investigations of (suitable) production terms and an extension of the simulations to void coalescence is planned for future studies.

Acknowledgements
It is a pleasure to mention the variety of friendly and fruitful discussions with Prof. W. Muschik, Dr. Ch. Papenfuss, and Prof. M. Ortiz (California Institute of Technology). Furthermore, the scholarship program of the Deutsche Bundesstiftung Umwelt (DBU) is gratefully acknowledged.

References

[1] Muschik, W., Papenfuss, C., Ehrentraut, H., A sketch of continuum thermodynamics, J. Non-Newton Fluid, 96 (2001), 255–290.
[2] Weinberg, K., Böhme, T., Mesoscopic modeling for continua with pores: application in biological soft tissue, J. Non-Equilib. Thermodyn., 33 (2008), 1–24.
[3] Belak, J., How metals fail, S&TR (from Lawrence Livermore National Laboratory), July/August (2002), 317–327.
[4] Takagi, K., Ishii, M., Crystal growth of sapphire filaments by a laser-heated floating zone technique, J. Mater. Sci. 12, (1977), 517–521.
[5] Xu, L., Pang, J.H.L., Interfacial IMC and Kirkendall void on SAC solder joints subject to thermal cycling, Proc. El. Pack. Tech. Conf., 2 (2005), 863–867.
[6] Tvergaard, V., Material failure by void growth to coalescence, Adv. Appl. Mech., 27 (1990), 83–151.
[7] Müller, I., Thermodynamics, p. 52, Pitman Advanced Publishing Program, Boston, 2001.
[8] Muschik, W., Papenfuss, C., Ehrentraut, H., Mesoscopic theory of liquid crystals, J. Non-Equilib. Thermodyn., 29 (2004), 75–106.
[9] Gross, D., Seelig, T., Fracture Mechanics, p. 244, Springer-Verlag, Berlin, 2006.
[10] Weinberg, K., Material Modeling of Microstructured Solids – Theory, Numeric and Applications, Habilitationsschrift, Ch. 6, p. 84, Technische Universität Berlin, 2006.
[11] Freund, L.B., Dynamic Fracture Mechanics, ch. 8, p. 442 ff., Cambridge University Press, Cambridge, 1998.

[12] Ortiz, M., Molinari, A., Effect of strain hardening and rate sensitivity on the dynamic growth of a void in a plastic material, J. Appl. Mech, 59 (1992), 48–53.
[13] Weinberg, K., Mota, A., Ortiz, M., A variational constitutive model for porous metal plasticity, Comput. Mech., 37 (2006), 142–152.
[14] Mercier, S., Molinari, A., Micromechanics of void growth at high rates, J. Phys. IV, 10 (2000), 415–420.
[15] Strachan, A., Cagin, T., Goddard, W.A., Critical behavior in spallation failure of metals, Phys. Rev. B, 63 (2001), 060103-1–060103-4.
[16] Voorhees, P.W., The theory of Ostwald ripening, J. Stat. Phys., 38 (1985), 231–252.

Paper received: 2007-04-11
Paper accepted: 2007-06-05